Self-pulsing in single section ring lasers based on quantum dot materials: Theory and simulations

Research Article | Vol. 26, No. 15 | 23 Jul 2018 | OPTICS EXPRESS 19044
Optics EXPRESS

Self-pulsing in single section ring lasers based on quantum dot materials: theory and simulations

LORENZO LUIGI COLUMBO,[1,2,*] PAOLO BARDELLA,[1] AND MARIANGELA GIOANNINI[1]

[1] *Dipartimento di Elettronica e Telecomunicazioni, Politecnico di Torino, Corso Duca degli Abruzzi 24, Torino, IT-10129, Italy*
[2] *Consiglio Nazionale delle Ricerche, CNR-IFN, via Amendola 173, Bari, IT-70126, Italy*
[*] *lorenzo.columbo@polito.it*

Abstract: We studied theoretically coherent phenomena in the multimode dynamics of single section semiconductor ring lasers with quantum dots (QDs) active region. In the unidirectional ring configuration our simulations show the occurrence of self-mode-locking in the system leading to ultra-short pulses (sub-picoseconds) with a terahertz repetition rate. As confirmed by the linear stability analysis (LSA) of the traveling wave (TW) solutions this phenomenon is triggered by an analogous of the Risken-Nummedal-Graham-Haken (RNGH) instability affecting the multimode dynamics of two-level lasers.

OCIS codes: (030.0030) Coherence and statistical optics; (140.4050) Mode-locked lasers; (140.5960) Semiconductor lasers; (190.4380) Nonlinear optics, four-wave mixing; (250.5590) Quantum-well, -wire and -dot devices.

References and links

1. K. Sato, "100 GHz optical pulse generation using Fabry-Perot laser under continuous wave operation," Electron. Lett. **37**, 763–764 (2001).
2. F. Lelarge, B. Dagens, J. Renaudier, R. Brenot, A. Accard, F. v. Dijk, D. Make, O. L. Gouezigou, J. G. Provost, F. Poingt, J. Landreau, O. Drisse, E. Derouin, B. Rousseau, F. Pommereau, and G. H. Duan, "Recent advances on InAs/InP quantum dash based semiconductor lasers and optical amplifiers operating at 1.55 μm," IEEE J. Sel. Top. Quantum Electron. **13**, 111–124 (2007).
3. J. Liu, Z. Lu, S. Raymond, P. J. Poole, P. J. Barrios, and D. Poitras, "Dual-wavelength 92.5 GHz self-mode-locked InP-based quantum dot laser," Opt. Lett. **33**, 1702–1704 (2008).
4. T. W. Hänsch, "Nobel lecture: Passion for precision," Rev. Mod. Phys. **78**, 1297–1309 (2006).
5. J. Faist, G. Villares, G. Scalari, M. Rösch, C. Bonzon, A. Hugi, and M. Beck, "Quantum cascade laser frequency combs," Nanophotonics **5**, 272–291 (2016).
6. T. J. Kippenberg, R. Holzwarth, and S. A. Diddams, "Microresonator-based optical frequency combs," Science **332**, 555–559 (2011).
7. P. J. Delfyett, S. Gee, M.-T. Choi, H. Izadpanah, W. Lee, S. Ozharar, F. Quinlan, and T. Yilmaz, "Optical frequency combs from semiconductor lasers and applications in ultrawideband signal processing and communications," J. Lightwave Technol. **24**, 2701–2719 (2006).
8. C.-H. Chen, M. A. Seyedi, M. Fiorentino, D. Livshits, A. Gubenko, S. Mikhrin, V. Mikhrin, and R. G. Beausoleil, "A comb laser-driven DWDM silicon photonic transmitter based on microring modulators," Opt. Express **23**, 21541–21548 (2015).
9. N. Eiselt, H. Griesser, M. H. Eiselt, W. Kaiser, S. Aramideh, J. J. V. Olmos, I. T. Monroy, and J.-P. Elbers, "Real-time 200 Gb/s (4x56.25 Gb/s) PAM-4 transmission over 80 km SSMF using quantum-dot laser and silicon ring-modulator," in "Optical Fiber Communication Conference," (2017), p. W4D.3.
10. S. M. Link, D. J. H. C. Maas, D. Waldburger, and U. Keller, "Dual-comb spectroscopy of water vapor with a free-running semiconductor disk laser," Science **356**, 1164–1168 (2017).
11. C. Gosset, K. Merghem, A. Martinez, G. Moreau, G. Patriarche, G. Aubin, A. Ramdane, J. Landreau, and F. Lelarge, "Subpicosecond pulse generation at 134 GHz using a quantum-dash-based Fabry-Perot laser emitting at 1.56μm," Appl. Phys. Lett. **88**, 241105 (2006).
12. Z. Lu, J. Liu, P. Poole, S. Raymond, P. Barrios, D. Poitras, G. Pakulski, P. Grant, and D. Roy-Guay, "An l-band monolithic InAs/InP quantum dot mode-locked laser with femtosecond pulses," Opt. Express **17**, 13609–13614 (2009).
13. P. Bardella, L. L. Columbo, and M. Gioannini, "Self-generation of optical frequency comb in single section quantum dot Fabry-Perot lasers: a theoretical study," Opt. Express **25**, 26234–26252 (2017).

#327447 https://doi.org/10.1364/OE.26.019044
Journal © 2018 Received 2 Apr 2018; revised 1 Jun 2018; accepted 16 Jun 2018; published 12 Jul 2018

Optics EXPRESS

14. L. L. Columbo, P. Bardella, M. Gioannini, Politecnico di Torino (Italy), "Spontaneous generation of frequency combs in QD lasers," Proc. SPIEE **10553**, 105530 (2018).
15. J. Faist, *Quantum Cascade Lasers*, (Oxford University Press, 2013).
16. N. Vukovic, J. Radovanovic, V. Milanovic, and D. L. Boiko, "Analytical expression for Risken-Nummedal-Graham-Haken instability threshold in quantum cascade lasers," Opt. Express **24**, 26911–26929 (2016).
17. A. Gordon, C. Y. Wang, L. Diehl, F. X. Kärtner, A. Belyanin, D. Bour, S. Corzine, G. Höfler, H. C. Liu, H. Schneider, T. Maier, M. Troccoli, J. Faist, and F. Capasso, "Multimode regimes in quantum cascade lasers: From coherent instabilities to spatial hole burning," Phys. Rev. A **77**, 1–18 (2008).
18. L. Lugiato, F. Prati, and M. Brambilla, *Nonlinear Optical Systems* (Cambridge University, 2015).
19. H. Risken and K. Nummedal, "Self pulsating in lasers," J. App. Phys. **39**, 4662–4672 (1968).
20. H. Choi, V.-M. Gkortsas, L. Diehl, D. Bour, S. Corzine, J. Zhu, G. Höfler, F. Capasso, F. X. Kärtner, and T. B. Norris, "Ultrafast Rabi flopping and coherent pulse propagation in a quantum cascade laser," Nat. Photonics **4**, 706–711 (2010).
21. M. Kolarczik, N. Owschimikow, J. Korn, B. Lingnau, Y. Kaptan, D. Bimberg, E. Scholl, K. Lüdge, and U. Woggon, "Quantum coherence induces pulse shape modification in a semiconductor optical amplifier at room temperature," Nat. Commun. **4**, 2953 (2013).
22. A. C. O. Karni, G. Eisenstein, V. Sichkovskyi, V. Ivanov, and J. P. Reithmaier, "Coherent control in a semiconductor optical amplifier operating at room temperature," Nat. Commun. **5**, 5025 (2014).
23. L. Liu, R. Kumar, K. Huybrechts, T. Spuesens, G. Roelkens, E.-J. Geluk, T. de Vries, P. Regreny, D. Van Thourhout, R. Baets, and G. Morthier, "An ultra-small, low-power, all-optical flip-flop memory on a silicon chip," Nat. Photonics **4**, 182–187 (2010).
24. Y. Wan, D. Jung, J. Norman, C. Shang, I. MacFarlane, Q. Li, M. J. Kennedy, A. C. Gossard, K. May Lau, and J. E. Bowers, "O-band electrically injected quantum dot micro-ring lasers on on-axis (001) GaP/Si and V-groove Si," Opt. Express **25**, 26853–26860 (2017).
25. S. Longhi and L. Feng, "Unidirectional lasing in semiconductor microring lasers at an exceptional point," Photon. Res. **5**, B1–B6 (2017).
26. C. C. Nshii, C. N. Ironside, M. Sorel, T. J. Slight, S. Y. Zhang, D. G. Revin, and J. W. Cockburn, "A unidirectional quantum cascade ring laser," App. Phys. Letters **97**, 231107 (2010).
27. Y. Barbarin, S. Anantathanasarn E.A.J.M. Bente, Y.S. Oei, M.K. Smit and R. Nötzel, "InAs/InP quantum dot Fabry-Perot and ring lasers in the 1.55 μm range using deeply etched ridge waveguides," Proceedings Symposium IEEE/LEOS Benelux Chapter, 2006, Eindhoven 137–140 (2006).
28. M. Rossetti, P. Bardella, and I. Montrosset, "Time-domain travelling-wave model for quantum dot passively mode-locked lasers," IEEE J. Quantum Electron. **47**, 139–150 (2011).
29. M. Gioannini, P. Bardella, and I. Montrosset, "Time-domain traveling-wave analysis of the multimode dynamics of quantum dot Fabry-Perot lasers," IEEE J. Sel. Top. Quantum Electron. **21**, 698–708 (2015).
30. A. Pérez-Serrano, J. Javaloyes, and S. Balle, "Bichromatic emission and multimode dynamics in bidirectional ring lasers", Phys. Rev. A, **81**, 043817 (2010).
31. L. Columbo and L. Gil, "Bistable self-starting pulses with terahertz repetition rate in a semiconductor microring laser", Opt. Lett. **35**, 1473–1475 (2010).
32. E. Roldán, G. J. de Valcárcel, F. Silva, and F. Prati, "Multimode emission in inhomogeneously broadened ring lasers," J. Opt. Soc. Am. B **18**, 1601-1611 (2001).
33. S. Koenig, D. Lopez-Diaz, J. Antes, F. Boes, R. Henneberger, A. Leuther, A. Tessmann, R. Schmogrow, D. Hillerkuss, R. Palmer, T. Zwick, C. Koos, W. Freude, O. Ambacher, J. Leuthold, and I. Kallfass, "Wireless sub-THz communication system with high data rate," Nat. Photonics **7**, 977–981 (2013).
34. S. Latkowski, F. Surre, and P. Landais, "Terahertz wave generation from a DC-biased multimode laser," App. Phys. Lett. **92**, 081109 (2008).
35. S. Latkowski, J. Parra-Cetina, R. Maldonado-Basilio, P. Landais, G. Ducournau, A. Beck, E. Peytavit, T. Akalin, and J.-F. Lampin, "Analysis of a narrowband terahertz signal generated by a unitravelling carrier photodiode coupled with a dual-mode semiconductor Fabry-Perot laser," App. Phys. Lett. **96**, 241106 (2010).
36. A. Pérez-Serrano, J. Javaloyes, S. Balle, "Longitudinal mode multistability in ring and Fabry-Perot lasers: the effect of spatial hole burning", Opt. Express **19**, 3284–3289 (2011).

1. Introduction

Semiconductor lasers operating in self-pulsing (SP) regime can be a simple alternative to passive and active mode-locked devices for the generation of high-repetition rate optical pulses [1–3]. In the frequency domain the SP regime corresponds to an Optical Frequency Comb (OFC), i.e a light emission characterised by equally spaced optical lines with low phase noise and low mode partition noise [4, 5]. These quite simple self-locked sources have attracted an impressive interest for applications in spectroscopy and in the rapidly growing field of high-capacity DWDM optical interconnection where the OFC laser diode feeds the silicon photonics optical modulators to

Optics EXPRESS

realize a compact and low cost transmitter [5–10].

As conventional Quantum Well (QW) based semiconductor lasers, more innovative active devices based on low dimensional materials as QDs and Quantum Dashes (QDashes) have now reached a quite high degree of technological development.

Experimental evidences of SP in single section Fabry-Perot (FP) lasers based on QDashes [11] and QDs [12] active materials have been reported. In the case of FP configuration we have recently demonstrated [13] that the carrier grating induced by the standing wave pattern (not washed out by diffusion) can explain the broad multi-wavelength optical spectra typically observed in QD lasers, whereas FWM allows the self-locking of the modes when the laser output power is high enough. Self-pulsing is predicted only in presence of saturable losses [14]. When SP occurs, the pulse repetition rate depends on the FP longitudinal cavity mode separation and for typical FP laser length it stays in the tens of gigahertz range.

The question remains on what happens if the standing wave pattern is not present, as for example in a ring laser configuration specifically designed to force only the clockwise (or counter clockwise) mode propagation. In this case, as shown by some recent works on Quantum Cascade Lasers (QCLs) that share with QD laser similar dynamical features [15–17], multi-wavelength emission and self-pulsation are triggered by a RNGH instability of the single mode TW. The RNGH instability consists in the parametric amplification of the cavity modes resonant with the frequency of the Rabi oscillations [18, 19].

The Rabi oscillations represent one of the most prominent effects of the coherent radiation-matter interaction regime in a two-level laser and give oscillations of the population inversion (and macroscopic medium polarization) at the Rabi frequency (ν_R), that is linearly proportional to the electric field strength and to the dipole moment, when (ν_R) is of the same order of the dephasing rate of the lasing transition. As happen for unipolar laser such as QCLs, where lasing action involves intersubband transitions, in high quality and narrow inhomogeneous broadening QD and QDash lasers the interband transitions between discrete levels are associated with quite narrow and symmetric gain linewidth (long dephasing time and low α-factor). This properties make this class of emitters similar to two-level lasers and thus it allows for the observation of coherent effects like Rabi oscillations. Rabi flopping in pulse propagation have been indeed measured in QCLs laser [20] and in QD semiconductor optical amplifiers at room temperature [21, 22] for a reasonable electric field strength. Hence, as already found in QCLs [17], we expect that also in QD and QDash unidirectional lasers the destabilization of the single model TW emission is caused by the RNGH instability [18, 19]. The latter can be considered the epitome of the self-mode-locking and SP in a two-level laser and, as anticipated above, occurs when longitudinal cavity modes that are resonant with the Rabi frequency get enough parametric gain to move above threshold. This means that Rabi frequency must be comparable (or close to a small multiple) of the cavity FSR, such that there exist one cavity longitudinal mode close to the Rabi frequency. From this follows that the predicted minimal laser length for the observation of the RNGH instability depends on the Rabi frequency at the instability threshold which in a two-level laser is proportional to the square root of the carriers relaxation rate [18]. Thus, while in solid state two-level lasers the minimal length corresponds to a very long cavity of tens of meters, in case of short carriers relaxation rates as in QCLs, QD and QDash lasers, it scales down to experimentally accessible values of hundreds of microns.

In [16] for example it is shown the Rabi frequency of QCLs is of the order of hundreds of gigahertz or few terahertz thanks to the the carriers relaxation time of $\simeq 1$ ps. Short cavity QCLs of few millimeters and the long emission wavelength of $\simeq 10\,\mu$m thus easily give a cavity FSR of the order of the Rabi frequency. In QD lasers, the carriers relaxation rate is also $\simeq 1$ ps or less, therefore we expect values of Rabi frequency similar to the QCL case. However, QD lasers of comparable length, emitting at shorter wavelengths of $\simeq 1\,\mu$m, have typical cavity FSR of the order of tens of gigahertz. This means that only one mode out of several modes can be

Optics EXPRESS

resonant with the Rabi frequency and probably it explains why in the FP cavity configuration, where we have shown that the carrier grating due to standing wave pattern is the main cause of destabilization of the single mode solution [13] by excitation of a band of adjacent longitudinal modes,Sato In more conventional bipolar semiconductor lasers based on QW active medium the Rabi oscillations and then consequently the RNGH instability are usually hindered due to the quite broad and asymmetric resonance (short dephasing time and high α-factor) and, to the best of our knowledge, not a single observation of these phenomena have been reported so far.

The aim of this paper is showing that a unidirectional QD ring laser (where standing wave patter carrier grating is eliminated) with low inhomogeneous broadening of the QD material gain is the ideal laser configuration for observing the RNGH instability and self-pulsing.

We note that semiconductor ring lasers and passive resonators are nowadays key elements for the realization of photonic integrated circuits [23] and in particular QD ring lasers integrated in a silicon photonic technology platform have been recently demonstrated in [24]. Unidirectional propagation can be easily guaranteed by a specific design (see for example [25, 26]).

We study in this paper the dynamical behaviour of an unidirectional QD ring laser of hundreds of microns length where multimode emission leads to SP as a result of a RNGH instability of the single mode TW solutions. We show that this phenomenon in unidirectional ring QD lasers is reliable on a wide range of bias currents and device lengths. As demonstrated in Section 3 as a consequence of the RNGH instability the SP repetition rate is in the hundred of gigahertz or few terahertz range, even if the ring cavity FSR is tens of gigahertz as in the standard FP laser configuration.

In order to simulate the multi-mode dynamics of the QD ring laser by properly taking into account coherent radiation-matter interaction we extended the Time Domain Travelling Wave (TDTW) model described in [28, 29] to include the temporal evolution of the medium polarization. The resulting TDTW model appear to be formally very close to the one previously used to study the pulse formation and multi-mode dynamics in two-level or in semiconductor bidirectional ring lasers [30, 31] although we will mostly concentrate here on unidirectional emission regime and on QDs gain material with inhomogeneous broadening.

We calculated the TW solutions of the system and we studied their stability against spatio-temporal perturbations with a standard Linear Stability Analysis (LSA) technique. As expected, the results of LSA show that the TW instability is associated with the amplification of the Rabi frequency in the QD active material that behaves as ensemble of artificial two-level atoms, thus having a RNGH character. Our numerical simulations show that the system spontaneously evolves towards a multimode solutions that corresponds to ultra-short pulses (hundreds of femtoseconds) at terahertz repetition rate, close to ν_R.

The numerical simulations also reveal that an increase of the degree of inhomogeneous broadening, that also represents an additional incoherent effect in the multi-mode competition, may reduce both the intervals of the bias current where SP is observed and the threshold of the RNGH instability in agreement with the results in [18, 32].

We finally observe that SP and the consequent OFC with terahertz or sub-terahertz optical line spacing can be desirable for a number of applications among which we mention the photonic generation of terahertz or sub-terahertz signals by illuminating a fast photodetector with the SP optical signal. This simple ring source could be therefore a valid alternative to the mixing of comb lines used nowadays to generate the terahertz signal [33–35].

To compare unidirectional and bidirectional configuration, we report the results obtained in a more standard bidirectional ring laser where we observed a much lower threshold current for the multimode emission; in the bidirectional case the multimode emission is in fact associated with Spatial Hole Burning (SHB) due to the standing wave pattern in the carriers density that cannot be washed out by diffusion in low dimensional active media such as QDs and QDashes [13]. Coherent dynamics leading to self-frequency comb generation is found for sizeable intervals of

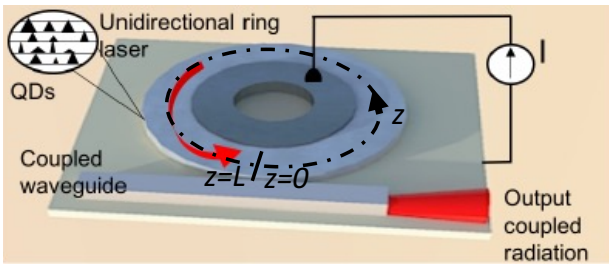

(a)

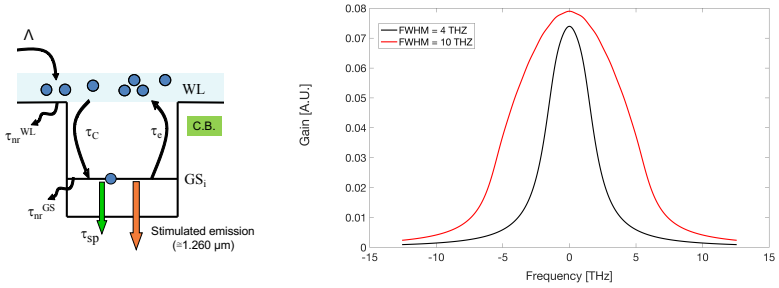

(b)

Fig. 1. (a) Sketch of the unidirectional ring configuration. (b) Schematic of the electron dynamics in an exemplary quantum dot sub-group i (left). Effective gain lineshape corresponding to inhomogeneous gain broadening of $\simeq 4$ THz ($\simeq 16$ meV) and $\simeq 10$ THz ($\simeq 40$ meV). The the FWHM of the homogeneous gain linewidth is $2\Gamma \simeq 2.4$ THz ($\simeq 10$ meV) corresponding to a dipole dephasing time of 130 fs (right). The zero frequency in the x-axis corresponds to $\omega_0/(2\pi)$.

the bias current, but it does not correspond to the emission of optical pulses. We find that while in the unidirectional case the optical lines of the comb have terahertz frequency spacing comparable with Rabi resonance, in the bidirectional case the spacing is the FSR of the ring cavity.

The paper is organised as follows: in Section 2, we describe the TDTW model used for simulating the multimode dynamics of the ring cavity single section QD laser. In Section 3, we present and discuss the results of the LSA of the TW solutions and in Section 4 those obtained by the numerical simulations for unidirectional and bidirectional InAs/GaAs QD laser. We draw our conclusions in Section 5.

2. Multi-populations time domain travelling wave model

We consider a single section Quantum-Dots-in-a-Well (DWELL) InAs/GaAs ring laser emitting from the ground state (GS) around 1258 nm [29]. The length of the laser cavity (L) is a few hundreds of microns. The laser structure with the coordinate system is sketched in Fig.1(a), whereas the QDs states, electron dynamics and gain line shapes for different inhomogeneous broadening are shown in Fig. 1(b).

We sketch in Fig. 1 the electron dynamics as taken in our model. The main material and device parameters are summarised in Table 2. The coherent interaction between QDs inhomogeneous broadened gain medium and the intracavity electric field is described trough a set of coupled traveling wave equations for the slowly varying envelop of the fundamental TE electric field

Optics EXPRESS

$E(z,t)$ and of the slowly varying envelop of the microscopic polarizations $p_i(z,t)$, coupled with the evolution equations for the electron occupation probabilities of ground state ρ_i in each dot group and in the wetting layer (WL) ρ_{WL} [29].

$$\frac{\partial E(z,t)}{\partial t} = \gamma_p \left(-\frac{\partial E}{\partial z} - \frac{\alpha_{wg} L}{2} E - C \sum_{i=-N}^{N} \bar{G}_i p_i + S_{sp}^{\pm} \right) \quad (1)$$

$$\frac{\partial p_i(z,t)}{\partial t} = (j\delta_i/\Gamma - 1) p_i - D(2\rho_i - 1)E \quad (2)$$

$$\frac{\partial \rho_i(z,t)}{\partial t} = -\rho_i \gamma_e (1 - \rho_{WL}) + F \rho_{WL} \gamma_C (1 - \rho_i) - \gamma_{sp} \rho_i^2 - \gamma_{nr}^{GS} \rho_i + H\, Re\,(E^* p_i) \quad (3)$$

$$\frac{\partial \rho_{WL}(z,t)}{\partial t} = \Lambda \tau_d - \gamma_{nr}^{WL} \rho_{WL} + \sum_{i=-N}^{N} \left[-\bar{G}_i \rho_{WL} \gamma_C (1 - \rho_i) + \frac{\bar{G}_i}{F} \rho_i \gamma_e (1 - \rho_{WL}) \right]. \quad (4)$$

In the convenient adimensional formulation provided by Eqs. (1)-(4) we scaled time to the fastest time scale in the system represented by the dipole dephasing time τ_d and the longitudinal coordinate to the cavity length L. The complex dynamical variables are linked to the corresponding physical quantities by the relations:

$$E \longrightarrow E \sqrt{\frac{\eta}{\Gamma_{xy}}} \frac{d_{GS}}{\hbar \Gamma}, \quad p_{0,i\,GS} \longrightarrow j\, p_{0,i\,GS} \sqrt{\frac{\eta}{\Gamma_{xy}}} \frac{N_D d_{GS}^2}{\epsilon_0 \hbar \Gamma h_{QD}}$$

where d_{GS} is the dipole matrix element associated with the optical transition from ground level, η is the effective refractive index, Γ_{xy} is the transverse optical confinement factor in the total QD active region, $\Gamma = 1/\tau_d$, h_{QD} is the QDs layer thickness, N_D is the number of QDs per unit area. The adimensional parameters C, D, F, H have the following expressions:

$$C = \frac{\omega_0 L \Gamma_{xy} \mu}{2c\eta},\ D = \frac{d_{GS}^2 N_D}{\epsilon_0 \hbar \Gamma h_{QD}},\ F = \frac{D_{WL}}{\mu N_D}, H = \frac{\tau_{sp} \Gamma^2 \omega_0 \Gamma_{xy} \hbar \epsilon_0 h_{QD}}{\eta \omega_{i\,GS} d_{GS}^2 N_D}$$

where ω_0 is our reference angular frequency coincident with the cold cavity mode closest to the GS gain peak, μ is the degeneracy of the ground state, $\omega_{i\,GS}$ is the transition frequency of the i group so that $\delta_i = \omega_{i\,GS} - \omega_0$, D_{WL} is the number of WL level per unit area per QDs layer and τ_{sp} is the spontaneous electrons decay time from the GS state. Moreover in the previous equations α_{wg} represents the wave guide losses, $\gamma_p = \tau_d v_g / L$ is the normalized photon decay rate, $\gamma_{e,C} = \tau_d / \tau_{e,C}$ are the normalized escape and capture rates, $\gamma_{sp} = \tau_d / \tau_{sp}$, $\gamma_{nr}^{WL,GS} = \tau_d / \tau_{nr}^{WL,GS}$ represent the normalized nonradiative decay rates and λ is the carriers injection probability per unit time. Finally $\bar{G}_i$ is the probability that a QD belong to the sub-group i and it follows a Gaussian distribution. Finally the noise source term due to spontaneous emission has the expression [28]: $S_{sp}^{\pm} = e^{i\phi_{sp}} \frac{d_{GS}}{\hbar \Gamma} \sqrt{\frac{\beta_{sp} N_D \bar{G}_i \mu \eta_L}{c \epsilon_0 \tau_{sp}} \sum_{i=-N}^{N} \left(\hbar \omega_{i\,GS} \rho_i^2 \right)}$ where β_{sp} represents the spontaneous emission factor accounting for the coupling between the spontaneously emitted radiation and the fundamental transversal guided mode. ϕ_{sp} is a random phase with uniform distribution in the range 0-2π. We chose for β_{sp} typical values between 10^{-2} and 10^{-3}.

In the unidirectional ring configuration the field envelope satisfies the boundary condition:

$$E(0,t) = \sqrt{1 - k^2} E(L,t),$$

where k is the output coupling coefficient between the ring and the coupled waveguide (see Fig. 1(a)). In this work we adopt periodic boundary conditions ($k = 0$) to be in the same

Optics EXPRESS

Table 1. Main materials and device parameters used in the TDTW model.

Symbol	Description	Values
	Material parameters	
η	Effective refractive index	3.34
μ	Confined states degeneracy	2
$1/\Gamma$	Dipole dephasing time	130 fs
d_{GS}	Dipole matrix element for GS	0.6 eV nm
τ_C	Electron capture times	1 ps
τ_e	Electron escape times	1.5 ps
τ_{nr}^{WL}	Electron non-radiative decay times	1 ns
τ_{nr}^{GS}	Electron non-radiative decay times	few ns
τ_{sp}	Electron spontaneous emission time	2 ns
	Device parameters	
w	Ridge width	5 µm
n_L	Number of QD layers	15
N_D	QD surface density	2.7×10^{10} cm^{-2}
D_{WL}	Wetting layer electron levels surface density	2.1×10^{11} cm^{-2}
h_{QD}	QD layer thickness	5 nm
α_{wg}	Intrinsic waveguide losses	4 cm^{-1}
k	Coupling coefficient	0
L	Device length	200 µm
Γ_{xy}	Transverse optical confinement factor	12 %

case considered in [18, 19] for the derivation of the RNGH instability. However the described phenomena, and in particular the existence of self-pulsing in the system, remain valid even for more realistic value of k as far as the photon life time remains much bigger than the dipole dephasing time (good cavity limit) [18].
Considering our normalisation and the physical constants, the output power, expressed in milliwatts, can be obtained by multiplying $|E(z,t)|^2$ by a factor of about 35. Finally, for sake of simplicity, we limit ourselves to the case where emission only occurs from the ground state [29].

3. Risken-Nummedal-Graham-Haken instability

To study the character of the TW instability we performed as reported in this section a semi-analytical linear stability analysis. This analysis requires first the calculation of the TW solutions, i.e. the single frequency solutions of Eqs. (1)-(4) (as detailed in paragraph 3.1) and then the evaluation of the stability against spatio-temporal perturbations of this solutions by calculating the perturbations parametric gain (as detailed in paragraph 3.2).

3.1. TW solutions

We looked for the single frequency solution of Eqs. (1)-(4) detuned in general by a quantity $\delta\omega$ from the gain peak ω_0 in the form

$$E = \overline{E} e^{j(\delta\omega/\Gamma\, t - \delta k\, Lz)}, \quad p_i = \overline{p_i} e^{j(\delta\omega/\Gamma\, t - \delta k\, Lz)}$$

$$\rho_i = \overline{\rho_i}, \quad \rho_{WL} = \overline{\rho_{WL}}$$

where we set $\delta k = \delta\omega/v_g$ and we introduced the group velocity $v_g = c/\eta$. This led to:

$$\overline{p_i} = \frac{\left[D(2\overline{\rho_i} - 1)\overline{E}\right]}{j\delta_i/\Gamma - 1 - j\delta\omega/\Gamma} \tag{5}$$

$$\overline{\rho_{WL}} = \frac{\Lambda\tau_d + \frac{1}{F}\sum_{i=-N}^{N} \bar{G}_i \overline{\rho_i}\gamma_e}{\gamma_{nr}^{WL} + \sum_{i=-N}^{N} \bar{G}_i \gamma_C (1 - \overline{\rho_i}) + \frac{1}{F}\sum_{i=-N}^{N} \bar{G}_i \overline{\rho_i}\gamma_e} \tag{6}$$

Optics EXPRESS

$$0 = \overline{E}\left(\frac{\alpha_{wg}L}{2} + C\,D\sum_{i=-N}^{N}\bar{G}_i\frac{(2\overline{\rho_i},-1)}{j\delta_i/\Gamma - 1 - j\delta\omega/\Gamma}\right) \quad (7)$$

$$0 = -\overline{\rho_i}\gamma_e(1-\overline{\rho_{WL}}) + F\overline{\rho_{WL}}\gamma_C(1-\overline{\rho_i}) - \gamma_{sp}\overline{\rho_i}^2 + H\,DRe\left(\frac{|\overline{E}|^2(2\overline{\rho_i}-1)}{j\delta_i/\Gamma - 1 - j\delta\omega/\Gamma}\right), \quad (8)$$

while in presence of inhomogeneously broadened gain and therefore multiple populations the TW solution can be found only by numerically solving the implicit nonlinear equations (5)-(8), in case of perfect homogeneous medium (i.e. only one population considered, $i = 1$) the TW equations (5)-(8) have an analytical solution.

3.2. Linear stability analysis of the TW solutions

The LSA of Eqs. (1)-(4) around the TW solutions is carried out in detail in Appendix A. The parametric gain, i.e. the maximum of the real part of the perturbation eigenvalue λ at a frequency $\nu_z = \omega_z/2\pi = k_z\, v_g/2\pi$ relative to the TW frequency treated as continuous variable, is plotted for example in Fig. 2. The cold cavity modes are those indicated by the dashed lines. We observe that the TW is unstable for $I \geq 55$ mA where a positive parametric gain favour the exponential growing of the modes with $k_{\mp 3} = \mp 3 \times 2\pi\,/L$. For lower currents in fact the parametric gain for all the cold cavity modes is negative.

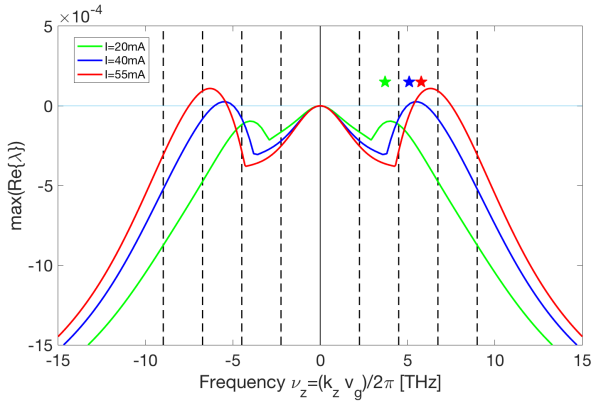

Fig. 2. Results of the LSA of the TW solutions for different bias currents. Plot of the parametric gain for each value of the frequency $\nu_z = \omega_z/2\pi = k_z\, v_g/2\pi$ treated as continuous variable. Dashed lines indicate the frequencies corresponding to the first values of k_z compatible with the periodic boundary conditions. We consider 3 QDs populations resonant with the lasing light associated with central angular frequencies 0, 1.0 THz and −1.0 THz that lead to a FWHM of the effective inhomogeneous broaden gain linewidth of $\simeq$ 4 THz ($\simeq$ 16 meV) (see Fig. 1). The other parameters are those used in [29]. The symbols indicate the position of the Rabi frequencies estimated using Eq. (9) closest to the parametric gain peak.

As shown in Fig. 2 we verified that the instability starts by developing Rabi sidebands around the TW lasing frequency and it can be seen as an amplification of the Rabi oscillations, in this sense it can be interpreted as a RNGH instability affecting the TW solutions in multimode two-level atoms [18]. In agreement with the results in [18] we found that the RNGH instability threshold is around 10 times the lasing threshold that in our case is $\simeq$ 5 mA.

The calculation of the Rabi frequency $\nu_R = \omega_R/2\pi$, associated to periodic exchange of energy between light and matter of the system, is reported in the following paragraph and is based on

Optics EXPRESS

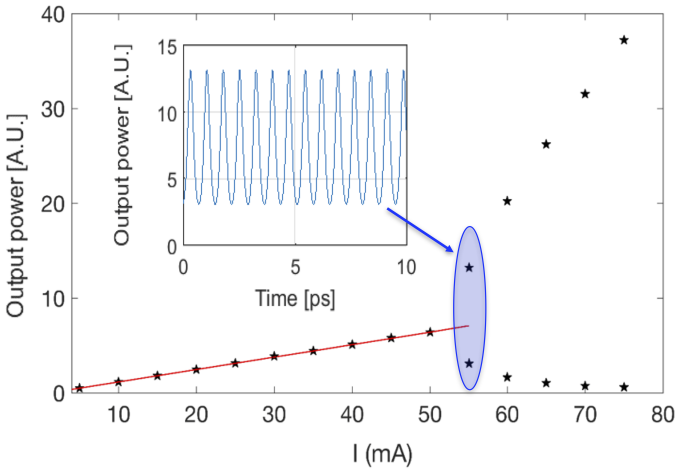

Fig. 3. Bifurcation diagram of the TW solutions: the maxima and minima in the output power time traces are reported against the bias current as control parameter. Red lines correspond to the TW solutions calculated using Eqs. (5)-(8).

the very well justified hypothesis that the QDs active medium is analogous to an ensemble of artificial two-level atoms.

Using the standard method described for example in [18] we calculate the Rabi frequencies associated with the each group of QDs of the multi-population ensemble:

$$\nu_{R,i} = \left(\gamma_{sp} H D 2|E|^2 + ((\delta_i - \delta\omega)/\Gamma)^2\right)^{0.5} /2\pi. \tag{9}$$

The large value of the ν_R, that turns out to be of the order of the inverse of the coherence time $(1/\Gamma)$ may also explain the recent experimental observations of Rabi oscillations effect in intense pulse propagation in QDs based SOA at room temperature [21, 22].

4. Results of dynamical simulations

We integrate the TDTW model equations using a finite difference algorithm as described in [13, 29].

For the parameters in Table 2 we obtained the bifurcation diagram in Fig. 3 where the maxima and minima in the output power time traces are reported versus the bias current as control parameter. Red lines correspond to the TW solutions calculated using Eqs. (5)-(8). As predicted by the linear stability analysis, for $I \geq 55$ mA the TW solution becomes unstable. In particular the multimode competition gives rise to regular power oscillations. The number of excited modes and the pulse contrast both increase with bias current. In Fig. 4 we report for example the temporal evolution of the output power, the optical spectrum and RF spectrum for $I = 75$ mA. In this case the first unstable mode has a distance of approximately 3 times the cavity FSR ($\simeq 440$ GHz) with respect to the TW emission frequency as shown in Fig. 4 (d) and, in perfect agreement with the results of the LSA in Fig. 2, it corresponds to the first lasing mode with a positive parametric gain. The side mode suppression ratio (SMSR) defined here as the ratio between the maximum RF peak power to that of the highest adjacent longitudinal modes is $\simeq 60$ dB. Moreover, because of the amplitude character of RNGH instability [18], the phases of the first excited longitudinal modes are locked with equal phase difference between adjacent modes. Once the first side modes are activated, a cascaded Four Wave Mixing (FWM) mechanism comes into play in fixing the

Optics EXPRESS

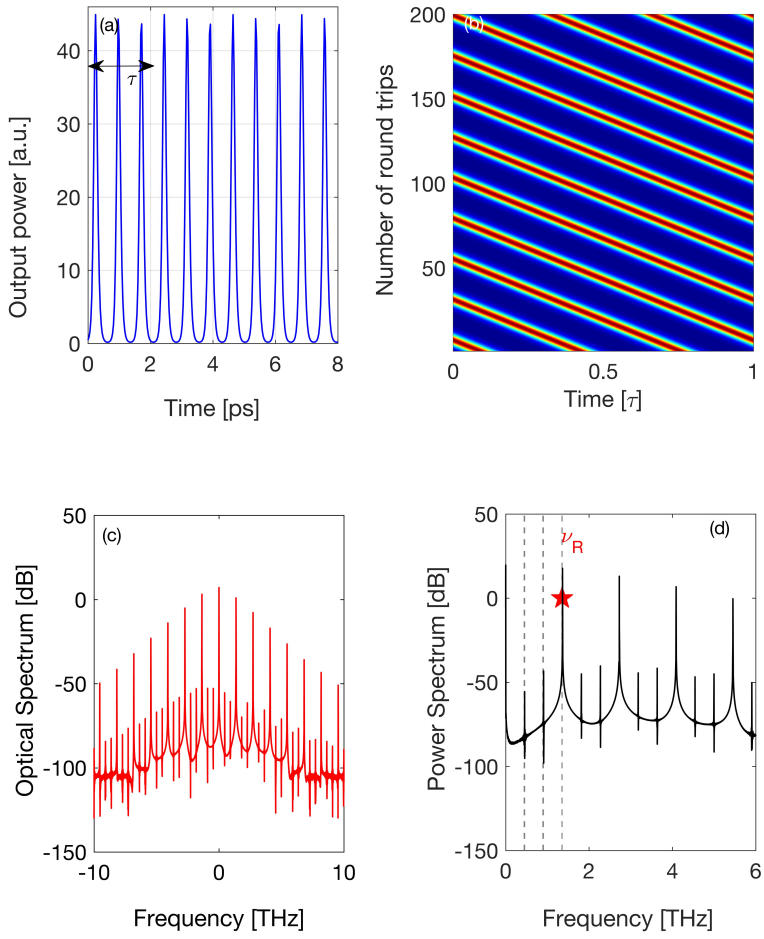

Fig. 4. Temporal evolution of the output power (a,b), optical spectrum (c) and RF spectrum (d) obtained for a value of bias current of 75 mA. In panel (b) we report a space-time representation of the pulse dynamics for 75 mA. A long time trace is divided in intervals corresponding to the cold cavity round trip time $\tau = L\eta/c$ (indicated in panel (a)). These segments are then stacked on top of each other so that the horizontal axis is equivalent to space inside the cavity while the vertical dimension describes the evolution in units of round trips. The lowest frequency dashed line in panel (d) corresponds to the ring resonator FSR (equal to $\simeq 440$ GHz), while the other two dashed lines are integer multiple of it. The other parameters are those used in Fig. 2.

frequency and the phase of the parametrically generated modes, thus yielding to the emission of ultra-short pulses at terahertz emission rate (see Fig. 4(a)). In the useful spatio-temporal representation in Fig. 4(b) three pulses are associated with a single cold cavity round trip time $\tau = L\eta/c$. As expected by the results of the LSA and shown for example in Fig. 5, the increase of the bias current allows us to partially tune the pulse repetition rate by changing the parametric gain peak position, or equivalently, the Rabi frequency of the system. In order to demonstrate the robustness of the SP phenomenon against ring length and current variation we run a set of systematic simulations. Our results might be conveniently summarised in Fig. 6 as a function of

Optics EXPRESS

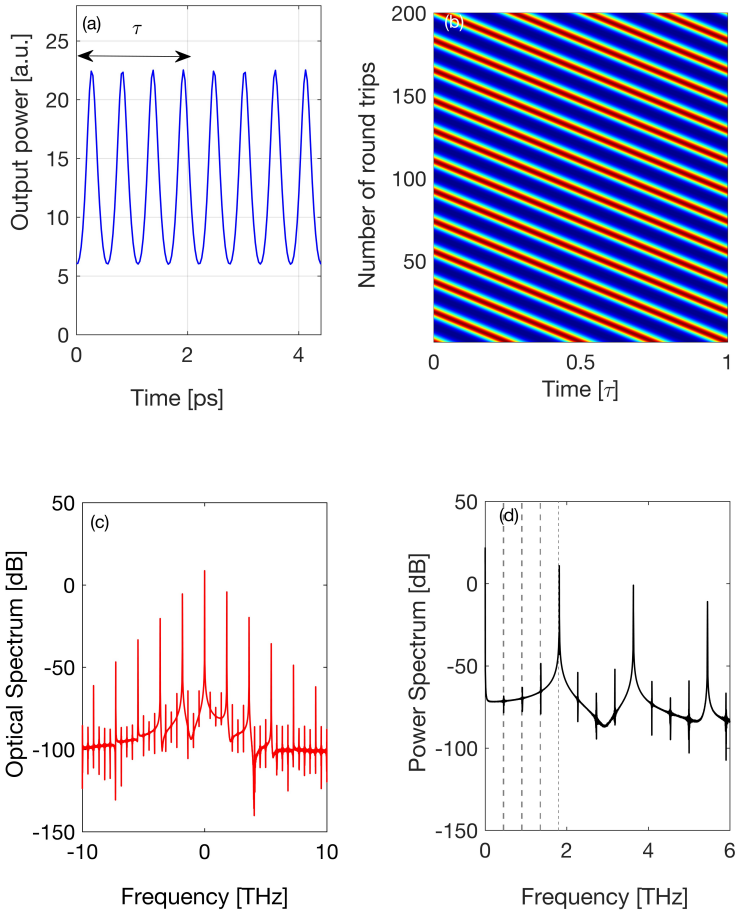

Fig. 5. Temporal evolution of the output power (a,b), optical spectrum (c) and RF spectrum (d) obtained for a value of bias current of 95 mA. Dashed lines in panel (d) denote the first cold cavity modes. The other parameters are those used in Fig. 4.

the cavity length L and the bias current I. In Fig. 6(a) we map the frequency of the RF peak (that turns to be always close to the Rabi frequency ν_R). In Fig. 6(b), in order to evaluate the spectral purity of the pulsed terahertz signal, we report the ratio between the power of the RF peak and the RF power of the competing adjacent RF lines corresponding to the ring modes not triggered by the RNGH instability. We define this ratio in the RF spectrum as SMSR (see Fig. 4(d)). It is possible to identify at least four different dynamical behaviour. In the great part of region A we have no pulsing with only one lasing line and CW power (TW stable). In the region denoted by the letter B the QD ring laser shows SP at a frequency in the terahertz range close to Rabi resonance, in the region denoted by the letter C phase-locking still induces regular oscillations although the emergence of side modes introduces pulse over-modulation, and finally in the region denoted by the letter D the multimode dynamics leads to irregular oscillations.

The impact of the inhomogeneous gain broadening on the observed RNGH instability is quantified in Fig. 6(c) and Fig. 6(d). In particular our simulations show that an increase of the inhomogeneous broadening in the model has a fundamental role in both lowering the threshold current of the RNGH instability (that in case of homogeneously broadened medium is around 10

Optics EXPRESS

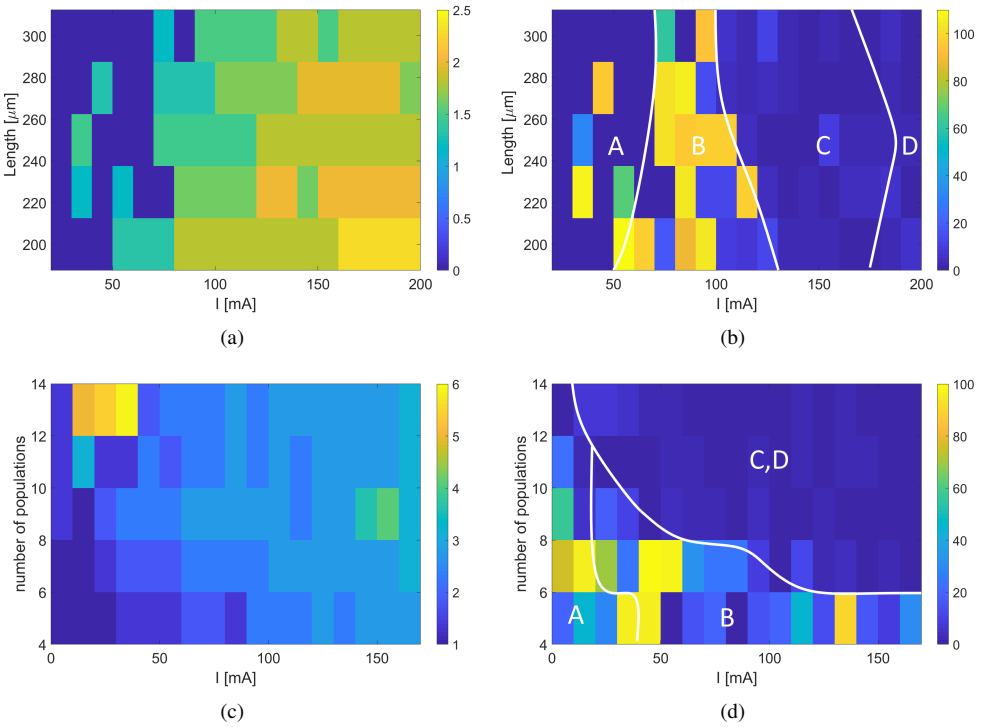

Fig. 6. Colour map representation of the frequency corresponding to the absolute maximum in the RF spectrum ($\nu \neq 0$), always close to ν_R, and the ratio between its amplitude and that of the highest side mode as a function of the cavity length L and the bias current I (a,b) or as a function of the degree of inhomogeneous broadening (number of populations) that ranges from a FWHM of ≃5.5 THz (≃22 meV) to a FWHM of ≃10.5 THz (≃42 meV) and the bias current I for a fixed cavity length $L = 200\,\mu$m (c,d). The other parameters are those used in Fig. 4.

times the lasing threshold), and expanding the band of unstable cavity modes for a given bias current. These results can be explained by the fact that inhomogeneous broadening increases the material gain of longitudinal modes non resonant with the Rabi frequency and they are in good agreement with those reported in [18, 32] for a two-level laser. This increment of unstable modes not necessarily indicates a broadening of region B (i.e. SP regime) since it also introduces a degree of incoherence in the system letting different lasing cavity modes to interact with different populations and than it might also lead to an expansion of the regions C and D of unstable pulses (see Fig. 6(c) and Fig. 6(d)). As an example we plot in Fig. 7 the results obtained by considering 11 populations whose central emission frequencies are separated by 1 THz and that correspond to a FWHM of the effective inhomogeneous broaden gain linewidth of ≃ 10 THz (≃ 40 meV) (see Fig.1), while keeping the other parameters as those in Fig. 4. In this case we observe an irregular temporal evolution of the output power, all the modes at the cavity FSR are turn above threshold. Examining the temporal evolution of the power and of the differential phase $\Delta\phi$ of all the optical lines we report a much higher differential phase and amplitude noise (see Fig. 8).

Optics EXPRESS

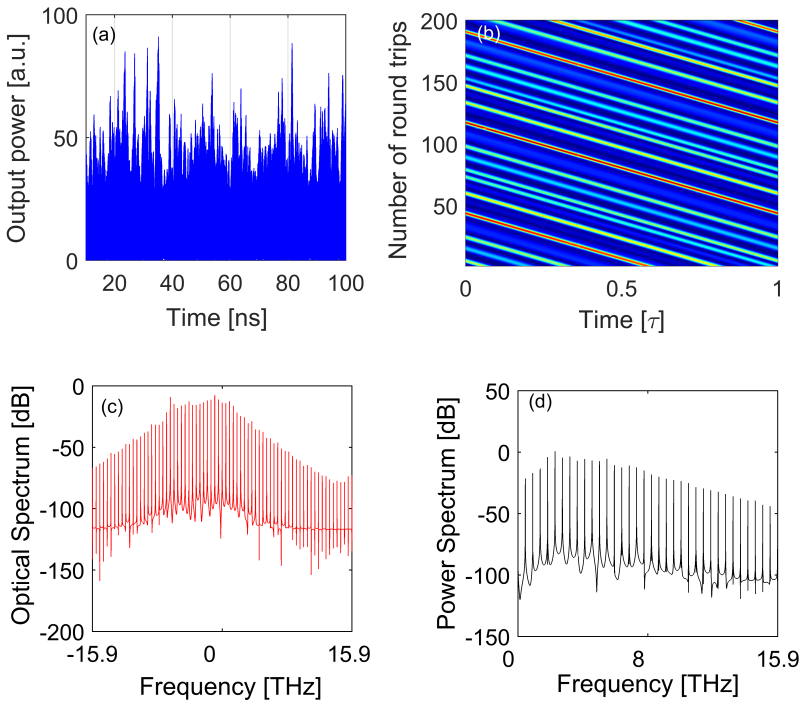

Fig. 7. Temporal evolution of the output power (a,b), optical spectrum (c) and RF spectrum (d) obtained for a value of bias current of 75 mA. We consider 11 QDs populations whose central emission frequencies are again separated by a 1 THz. The other parameters are those used in Fig. 4.

4.1. *Bidirectional ring*

We finally observe that in the bidirectional configuration, the standing wave pattern due to the interference between forward and backward fields generates a grating in the carrier density that cannot be washed out by diffusion. Equations for the first Fourier components of the spatial grating are added following the procedure described in [13]. Spatial Hole Burning takes place, letting the TW instability threshold decrease from several times the lasing threshold down to a few percents above the lasing threshold. This emerges for example from inspection of Fig. 9 where, focusing on the simple case of a single QD population (homogeneous gain broadening), we report the linear stability analysis of the TW solutions for a bidirectional configuration (panel a) and a unidirectional one (panel b). The latter has been carried on via a calculations analogous to that described in [16, 17] in the case of a QCLs. In the unidirectional configuration only the mode at 0 THz has positive parametric gain (see Fig. 9(a)); all the others are suppressed and only by increasing current the two relative maxima at $\simeq \pm 1.2$ THz will experience positive parametric gain and they will allow the lasing of the modes closer to these two maxima. Instead, in the bidirectional ring configuration all the cavity modes in the frequency range of few terahertz experience a positive parametric gain (see Fig. 9(a)) which is turned-on by the SHB effect. The TW resonant with the gain peak is unstable very close to the lasing threshold and by increasing the bias current we generally observe an alternation between regimes of irregular oscillations and a regular dynamical behavior as recently reported in [13]. Coherent dynamics leading to self-generation of OFCs with lasing lines spaced of the ring FSR is found for sizeable intervals of the bias current. It does not correspond to the emission of optical pulses (since the phase

Optics EXPRESS

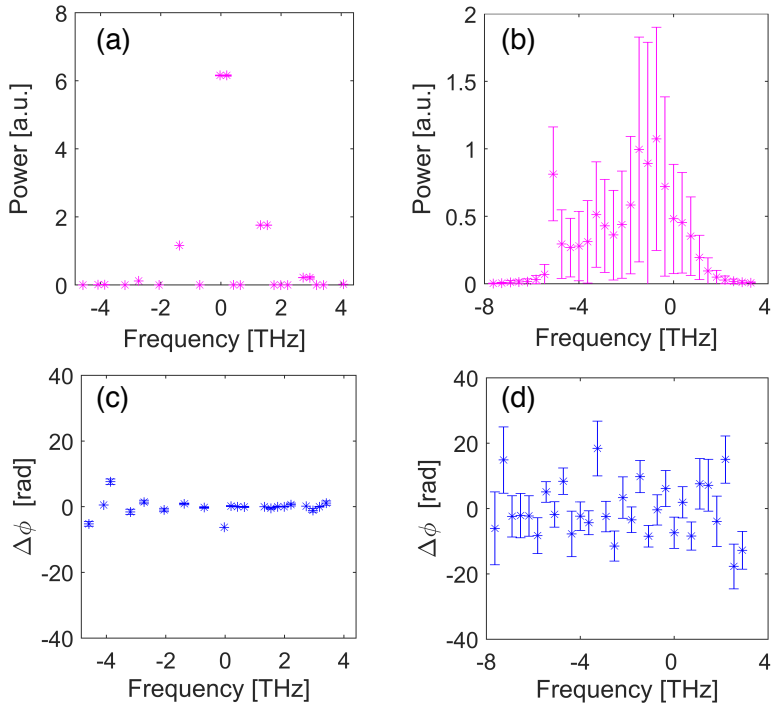

Fig. 8. Average values of the modal power and of the differential phase. The errors bars denote the standard deviation of their temporal fluctuations in the case of 3 (a), (c) and 11 populations (b), (d). The other parameters are those used in Fig. 4.

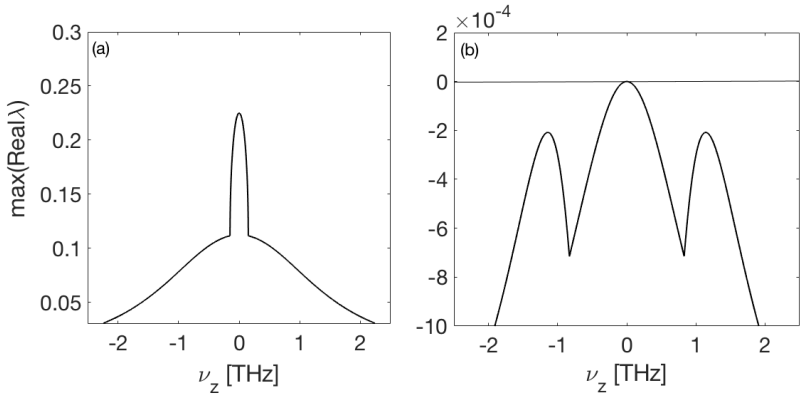

Fig. 9. Results of the LSA of the TW solutions for $I = 60\,\mathrm{mA}$ for a bidirectional ring configuration (a) and an unidirectional one (b). Plot of the parametric gain for each value of the frequency $\nu_z = \omega_z/2\pi = k_z\, v_g/2\pi$ treated as continuous variable. The other parameters are those used in Fig. 4.

difference between adjacent modes is not equal), although is normally associated to the emission of a broader and flatter optical spectrum. Although it was out of the scope of the present work we observe that we did not find phenomena of spontaneous unidirectional operation as those

Optics EXPRESS

studied in [36], probably because of a smaller diffusion characteristic of the QD active medium considered here.

5. Conclusions

We studied self-mode-locking and in particular self-pulsing in single section ring QD lasers. In unidirectional emission regime ultra-short pulses at terahertz repetition rate are triggered by RNGH multi-wavelengths instability of the TW solutions that consists in the amplification of the Rabi frequency of the system. The latter has been calculated in the very well verified hypothesis that radiation coherently interacts with QDs material as with an ensemble of artificial two level atoms. In bidirectional cavities, SHB makes the TW instability threshold occurring for much lower bias current, but only self-generation of OFCs is reported. Our results let envisage very timely applications such as the high-data rate optical information encoding and transmission or the generation of terahertz or sub-terahertz signals via combination of photonics and electronics.

6. Appendix A

We study the stability of the TW emission respect to spatio-temporal perturbations looking for solutions of Eqs. (1)-(4) in the form:

$$E = (\overline{E} + \delta E)e^{j(\delta\omega/\Gamma\, t - \delta k\, Lz)} \quad p_i = (\overline{p_i} + \delta p_i)e^{j(\delta\omega/\Gamma\, t - \delta k\, Lz)}$$

$$\rho_{WL}(z,t) = \overline{\rho_{WL}} + \delta\rho_{WL} \quad \rho_i(z,t) = \overline{\rho_i} + \delta\rho_i$$

This gives the following set of linear equations for the perturbations:

$$\frac{\partial \delta E}{\partial t} + \gamma_p \frac{\partial \delta E}{\partial z} = \gamma_p \left(-\frac{\alpha_{wg} L}{2} \delta E - C \sum_{i=-N}^{N} \bar{G}_i \delta p_i \right) \tag{10}$$

$$\frac{\partial \delta p_i(z,t)}{\partial t} = (j\delta_i/\Gamma - 1 - j\delta\omega/\Gamma)\delta p_i - D(2\delta\rho_i)E - D(2\rho_i - 1)\delta E \tag{11}$$

$$\begin{aligned} \frac{\partial \delta\rho_i(z,t)}{\partial t} &= -\delta\rho_i\gamma_e(1-\rho_{WL}) + \rho_i\delta\rho_{WL}\gamma_e - F\delta\rho_i\rho_{WL}\gamma_C \\ &+ F(1-\rho_i)\delta\rho_{WL}\gamma_C - 2\rho_i\delta\rho_i + H\,Re\,(\delta E^* p_i + E^*\delta p_i) \end{aligned} \tag{12}$$

$$\begin{aligned} \frac{\partial \delta\rho_{WL}(z,t)}{\partial t} &= -\delta\rho_{WL}\gamma_{nr}^{WL} + \sum_{i=-N}^{N} \Big[-\bar{G}_i\delta\rho_{WL}\gamma_C(1-\rho_i) \\ &+ \bar{G}_i\rho_{WL}\gamma_C\delta\rho_i + \frac{\bar{G}_i}{F}\delta\rho_i\gamma_e(1-\rho_{WL}) - \frac{\bar{G}_i}{F}\rho_i\gamma_e\delta\rho_{WL} \Big]. \end{aligned} \tag{13}$$

Projecting on the spatial Fourier basis the perturbations we derive for each perturbation wave vector k_n a set of ODE for the temporal evolution of the corresponding Fourier component. The maximum of the real parts of the eigenvalues λ of the associated Jacobian matrix (Lyapunov exponents), representing the parametric gain of the considered mode, thus give a direct information about the TW stability.